Demonstration of Real-Time, Phase-Locked Alignment of Tiled Gratings for Chirped-Pulse–Amplified Lasers

Introduction

The OMEGA EP (extended performance) petawatt, multikilojoule, solid-state laser, presently under construction at LLE, includes compressors with four tiled-grating assemblies (TGA's), where each assembly contains three subaperture diffraction gratings, to compress the pulse before it is focused onto target.[1,2] The tiled-grating compressor (TGC) was chosen to stay within the damage-threshold limitations of the largest currently available multilayer dielectric (MLD) gratings, together with the anticipated intensity modulation of the laser output beam. The four-grating compressor is shown schematically in Fig. 100.17. The holographically generated grating tiles[3,4] have a line frequency of 1740 grooves/mm and a clear aperture of 400 × 470 mm. The individual BK-7 grating substrates have a thickness of nominally 100 mm and are approximately 50 kg in weight. For the TGC to deliver the compressed pulse with a near-diffraction–limited energy distribution on target, the individual tiles have to be aligned to each other with an optical-path difference (OPD) of less than 50 nm. An active control approach, similar to a three-actuator deformable mirror, has been chosen to maintain the correct alignment between grating tiles.

Between any two gratings there are six degrees of freedom that affect the optical performance of a tiled-grating system, as shown in Fig. 100.18. A three-control-variables approach has been chosen to bring the gratings into the condition of coherent energy addition.[5] This reduction in degrees of freedom is realized by grouping six variables into three pairs that mutually compensate. Differential tilt, caused by small differences in the average groove spacing, is removed by adjusting the individual grating tilt. Also, error in lateral placement of the gratings is compensated for by a small adjustment of piston. In addition, error in groove parallelism between gratings is compensated by a *y*-tip adjustment. Although each differential error must be kept small, compensation between pairs allows all six degrees of freedom to be nonzero while coherent addition is maintained. Using this pairing concept, a systematic alignment sequence provides convergence toward accurate coherent addition.

Several new alignment techniques have been demonstrated to achieve coherent addition of tiled gratings. The relative grating positions and all alignment measurements are made in real-time with an interferometer whose field of observation straddles the gap between the gratings. Any drift of the grating tiles from their optimal position is measured and compensated by a servo loop. The gratings are pre-aligned to have a differential piston of less than 10 μm, which is the capture range of the servo system. With the servo loop engaged, an alignment

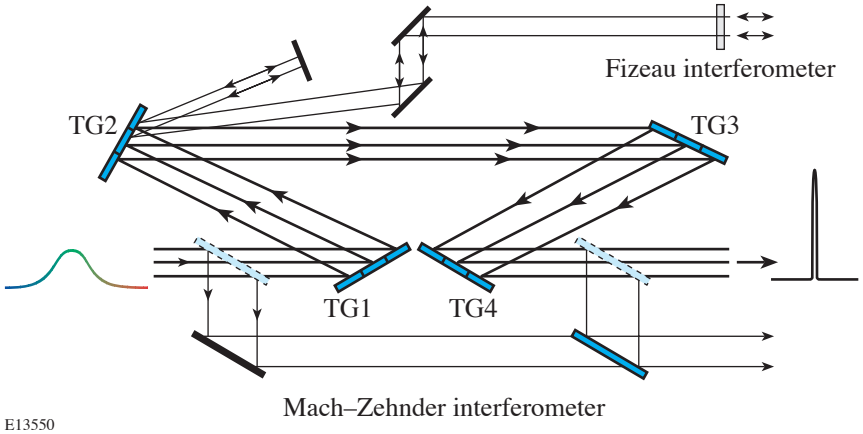

Figure 100.17
Each OMEGA EP compressor contains four tiled-grating assemblies (TGA's) per beamline, where each assembly contains three subaperture diffraction gratings. Each TGA interface requires three actuators to maintain the grating positioning needed for coherent addition of the three diffracting beams. The tiled-grating compressor (TGC) provides an aperture large enough to meet the energy requirements while operating below the laser-damage threshold of the final grating. Interferometers are deployed to maintain accurate alignment of the gratings within each TGA.

precision of ±25 nm, or λ/20 p–v, is reproducibly achieved. In addition, as schematically illustrated in Fig. 100.17, a robust alignment system, intended for use on the OMEGA EP laser system, contains two interferometers. Individual TGA's are aligned with a Fizeau interferometer, while alignment of the entire TGC is verified with a Mach–Zehnder interferometer and a focal-spot diagnostic.

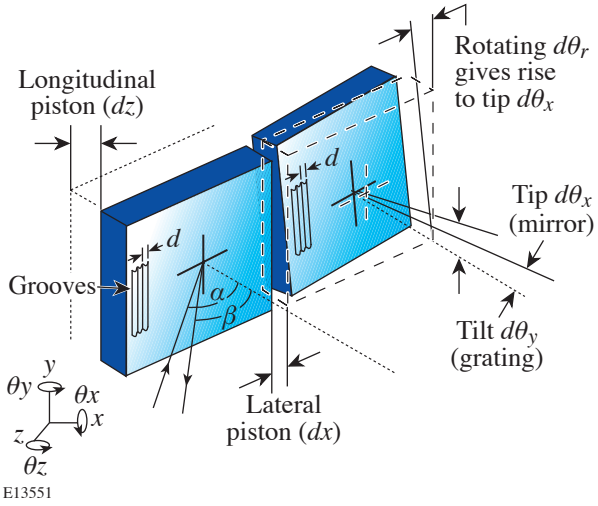

Figure 100.18
Between any two gratings there are six degrees of freedom that affect the optical performance of a tiled-grating system. These can be grouped into three compensating pairs of differential errors: longitudinal piston and lateral piston; in-plane rotation and angular tip; and average groove spacing and angular tilt. Although each differential error must be kept small, compensation between pairs removes the constraint that any particular error must be zero.

Modeling

A measure of the accuracy with which two gratings operate in the coherently additive mode is the Strehl ratio, which is defined as the ratio of the peak irradiance of an aberrated focal spot to that of an aberration-free focal spot.[6] Computer simulations of one TGA interface show the effect of the differential grating misalignments as measured in the near field. Tip, tilt, or piston misalignment between the gratings affects the Strehl ratio to different degrees for the same magnitude of alignment error. This sensitivity is shown for piston, *x* tilt, *y* tip, and in-plane rotation in Fig. 100.19, which plots the Strehl ratio as a function of a misalignment error. Although the TGC in the OMEGA EP laser system will operate at a wavelength of 1054 nm, both modeling and prototype development were carried out at a wavelength of 633 nm because of the availability of an interferometer operating at this wavelength. To achieve accurate tiling at either wavelength, the misalignment errors, taken individually or as compensation pairs, must be kept below λ/20 to maintain close to a diffraction-limited focal spot.

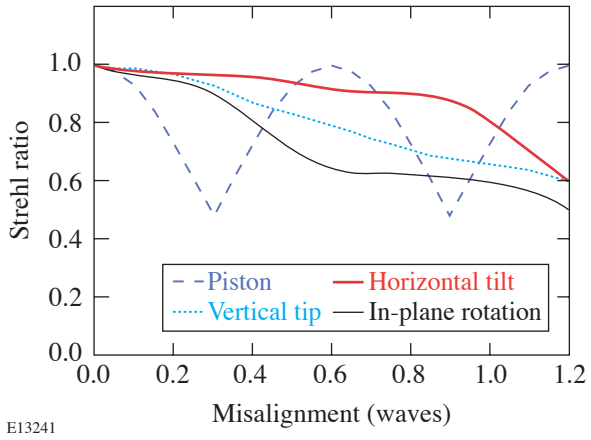

Figure 100.19
Computer simulations of one TGA interface show the effect of the differential grating misalignments as measured in the near field. The Strehl ratio is plotted as a function of individual misalignments for a wavelength of 633 nm and an incident angle of 33.4°. The misalignment errors, taken individually or as compensation pairs, must be kept below λ/20 to maintain close to a diffraction-limited focal spot.

These computer simulations show that piston is the most-sensitive drift parameter for two gratings and that the effects of piston error are cyclical with an OPD period of λ/2. Since the absolute piston error has to be less than one wavelength, any error must be corrected before it reaches λ/2; otherwise the absolute piston position can be lost due to a periodic π ambiguity. If the fringe system jumps by an error greater than λ/2, the piston must be reset independently and the tracking/correcting system restarted.

Three equations mathematically describe the paired relationship for the various degrees of freedom. Defining displacements as Δz (longitudinal piston shift), Δx (lateral piston shift), θx [rotation about *x* axis (tip)], θy [rotation about *y* axis (tilt)], θz [rotation about *z* axis (in-plane rotation)], and Δd (error in grating ruling spacing), the following three equations represent the resulting phase errors. Equation (1) represents the piston phase error while Eqs. (2) and (3) represent the phase gradients of tip and tilt, respectively, where $d\Phi/dy$ and $d\Phi/dx$ are the transverse phase gradients in the beam, α is the incident angle, and β is the diffraction angle. The objective for accurate tiling involves setting each equation to zero for the majority of spectral components of the laser pulse.

$$\Delta\Phi_z = 2\pi/\lambda\left[(\sin\alpha + \sin\beta)\Delta x - (\cos\alpha + \cos\beta)\Delta z\right]. \quad (1)$$

$$d\Phi/dy = -2\pi/\lambda\left[(\cos\alpha + \cos\beta)\theta_x + (\sin\alpha + \sin\beta)\theta_z\right]. \quad (2)$$

$$d\phi/dx = 2\pi/\lambda\left[(\cos\alpha + \cos\beta)\theta_y - (\sin\alpha + \sin\beta)\Delta d/d\right]\sec\beta. \quad (3)$$

Three independent actuators that produce displacements normal to the surface of the grating are used to control differential tilt, tip, and piston. The motion of a single actuator rotates the grating about an axis defined by the other two actuators. This rotation is resolved into tilt and tip components by projection of the axis onto the coordinate system axes. Piston displacement is simply the corresponding normal displacement of the grating surface at a reference point selected for piston measurement. It is convenient to combine the coefficients for tip, tilt, and piston motion due to actuator displacements into a 3 × 3 matrix M and to calculate its inverse M^{-1}, which is also a 3 × 3 matrix. Then the actuator motions required to produce a specified tilt, tip, and piston correction are described by $Z = M^{-1}C$, where Z is the row vector of required actuator displacements and C is the column vector of tilt, tip, and piston corrections.

Experimental Setup

Several different prototype assemblies were built to study error compensation, TGA-to-TGA compensation schemes, and various alignment techniques. The tiled-grating mounts are identical three-point, flexure suspensions that separate weight-bearing and adjustment functions, as shown in Fig. 100.20. The front view of a prototype TGA shows two gold-coated, 16 × 22-cm gratings, manufactured by Jobin-Yvon, while the back view shows both the manual and motorized actuators. The entire TGA is mounted on a precision rotating stage to achieve rapid and repeatable angular adjustment when positioning to a normal, Littrow, or near-Littrow angle of incidence. The design emphasizes pre-loaded, easy motion in the direction of control while being very stiff in two orthogonal directions, thus minimizing parasitic motions.

The experimental test bed used to demonstrate closed-loop control of TGA's is configured on an optical table containing a Fizeau interferometer (Fig. 100.21), with an ADE Phase Shift Mini Fiz 100 front end, operating at 632.8 nm. The out-

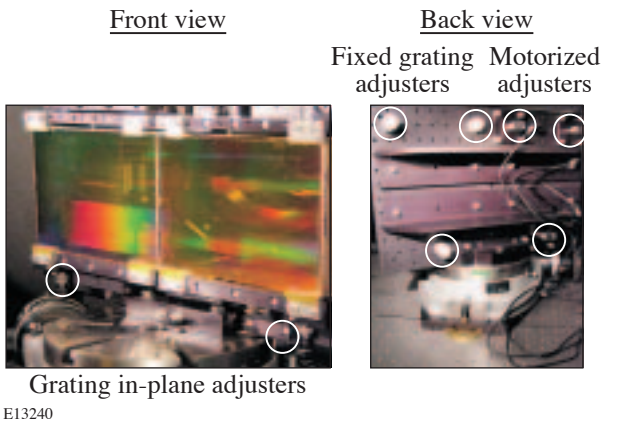

Figure 100.20
The front view of a prototype TGA shows two gold-coated, 16 × 22-cm gratings, while the back view shows both the manual and motorized actuators. The TGA is mounted on a precision rotating stage to achieve rapid and repeatable angular adjustment when positioning to a normal, Littrow, or near-Littrow angle of incidence. Several different prototype assemblies were built to study error compensation, TGA-to-TGA compensation schemes, and various alignment techniques.

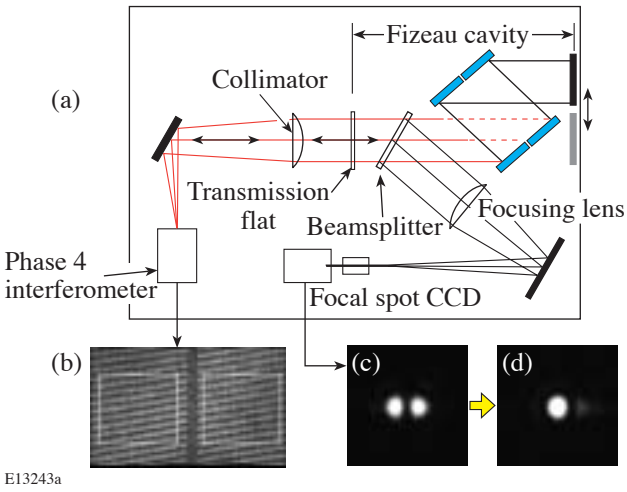

Figure 100.21
The experimental test bed used to demonstrate closed-loop control of tiled-grating assemblies (TGA's) is configured on an optical table containing a 10-in. Fizeau interferometer (a). The TGA's are positioned within the interferometer cavity for testing single- and double-pass alignment, using one TGA, or triple- and quadruple-pass alignment, using two TGA's. The fringe pattern (b) is a sample of a recorded interferogram, while (c) and (d) are examples of a piston phase error of $\lambda/2$ and a diffraction-limited focal spot, respectively.

put beam was expanded to 250 mm, using a 1.8-m-focal-length lens for collimation, as shown in Fig. 100.21. A 12-in.-diam transmission flat, manufactured by Zygo, was inserted into the Fizeau cavity to send a portion of the return beam for far-field analysis, as described previously.[7] The TGA's were positioned within the interferometer cavity for testing single- and double-pass alignment, using one TGA, or triple- and quadruple-pass alignment, using two TGA's. The fringe pattern [Fig. 100.21(b)] is a sample of a recorded interferogram, while Figs. 100.21(c) and 100.21(d) are examples of a piston phase error of $\lambda/2$ and a diffraction-limited focal spot, respectively.

One grating in the TGA was adjustable through remotely controlled piezo-type actuators (New Focus PicoMotors, model 8301)[8], while the second grating was held steady after manual adjustment with Aerotech Differential micrometers. The suspension mounts for both gratings were mounted on a common backplate. The backplate assembly was mounted on a 250-mm-diam rotary table with a resolution of 4 arc sec (manufactured by Phase II). Parallelism of the gratings' grooves was obtained by pivoting one of the gratings about the grating normal, while the TGA was alternately positioned at normal incidence and Littrow position within the Fizeau interferometer. After several iterations, grating parallelism was adjusted to within 0.1 wave. The functional systems diagram is shown in Fig. 100.22. The prototype control system monitors grating alignment in both the near field and far field (focal spot). The cw laser light probes the gratings and is transmitted to electronic cameras to record both the fringe pattern and the corresponding focal spot. Analysis of the fringe pattern yields differential tip, tilt, and piston. From these measurements, the system computer generates signals to drive three actuators, for each grating-to-grating interface, in a closed-loop cycle that minimizes the set of differential errors. The focal-spot diagnostic is used to verify successful convergence toward diffraction-limited performance.

Phase Measurement and Error-Signal Computation

Any drift between the two gratings is determined from a single interferogram according to a Fourier-transform (FT) method known as spatially synchronous phase detection (SSPD).[9] Figure 100.23 shows the methodology by which this technique is used to analyze the high-frequency fringe patterns situated on either side of the TGA interface. The interferometer is adjusted with deliberate tilt between the reference and test wavefronts to produce an interferogram [Fig. 100.23(a)] that contains the surface information encoded onto a high-order spatial carrier frequency. A window function is applied to remove edge-ringing [Fig. 100.23(b)]. The FT of the interferogram [Fig. 100.23(c)] produces a dc component and two sidebands symmetrically displaced corresponding to the carrier frequency of the fringe pattern. Higher-order sidebands are present with nonsinusoidal fringe profiles. Each of the sidebands contains all of the desired phase information. The carrier frequency is chosen to place the side lobe to a position outside the noise spectrum of the interferometer system. One sideband is isolated by applying an appropriate filter in the Fourier plane and shifted to zero frequency before carrying out the inverse Fourier transform. Two-dimensional phase reconstruction of each side of the TGA interface is obtained with an inverse FT, followed by calculation of the phase from the real and imaginary components of the image. The complex phase of the inverse transform is unwrapped and represents the phase data of the surfaces [Fig. 100.23(d)]. Any remaining tip, tilt, or

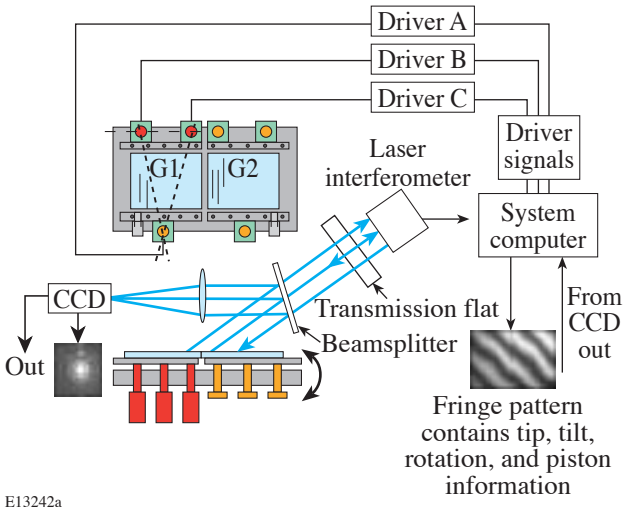

Figure 100.22
The control system monitors grating alignment in both the near field and far field (focal spot). The cw laser light probes the gratings and is transmitted to electronic cameras to record both the fringe pattern and the corresponding focal spot. Analysis of the fringe pattern yields differential tip, tilt, and piston. From these measurements, the system computer generates signals to drive three actuators in a closed-loop cycle that minimizes the set of differential errors. The focal-spot diagnostic is used to verify successful convergence toward diffraction-limited performance.

piston phase errors can be removed in the final stages of closed-loop operation. This technique is especially useful when operating in optically "noisy" environments since the single video frame measurement is fast compared to scanning interferometers and permits a high level of noise rejection, through averaging of multiple video frames in phase space.

The differential slope of the two elements represents the x tilt and y tip of the two tiles. The x tilt and y tip are determined unambiguously in the x–y coordinate system. "Piston" is the out-of-plane offset in the z direction. A linking of the left and right portions of the interferogram has to be applied across the gap to maintain phase continuity for the piston computation.

As previously described in this article, the three phase-error terms are the result of the joint effect of a pair of separate, independent grating misalignments. The piston term is the composite effect of both an actual z-direction tile offset and a lateral shift perpendicular to the grating rulings. The tip term comprises the joint effect of actual differential tip and in-plane rotation of one of the gratings with respect to the other. The tilt term is due to differential tilt between the gratings, which can, in part, be caused by a difference in groove spacing. An error in one of the components of a two-component term may be perfectly compensated by adjusting the other component; therefore, it is necessary to provide only three adjustments per tile, provided that the grating array is designed to minimize errors in the nonadjustable offsets.

After an initial system alignment where most of the tip and tilt have been removed and the relative piston has been set within $2\pi N$, the value of N is checked by translating a high-resolution mechanical indicator across the gap on the grating surface outside of the clear aperture. The indicator is mounted on a slide that is parallel to the surface of the first grating and that places the indicator within a few millimeters, laterally, of the gap. Translating the indicator while in contact with gratings produces a step if there is an absolute piston error. The three

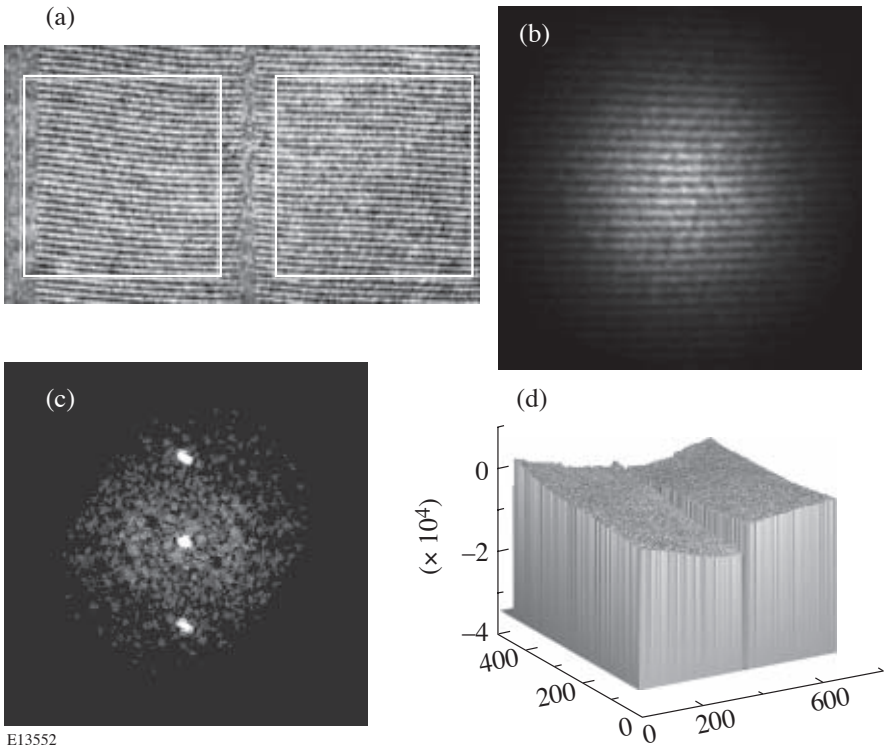

Figure 100.23
A Fourier-transform (FT)–based algorithm, referred to as spatial synchronous phase detection (SSPD), is used to analyze high-frequency fringe patterns (a) situated on either side of the TGA interface. A window function is applied to each fringe pattern (b) to reduce edge effects in the FT calculations. The carrier frequency is chosen to place the side lobe to a position outside the noise spectrum of the interferometer system (c). An inverse FT, followed by phase calculations, results in two-dimensional phase reconstruction of each side of the TGA interface. Any remaining tip, tilt, or piston phase errors (d) can be removed in the final stages of closed-loop operation.

actuators of the motorized gratings are now moved in concert by an appropriate amount to reduce the absolute piston to less than one wavelength.

Computer System and Software

The software integrates the image acquisition, image analysis, parameter derivation, and actuator control, as well as all data logging, in the same computer. The speed of the control loop is of the order of 1 s, even though the actual alignment may be corrected much less frequently. For the purpose of thorough testing, the measurement system was designed to be sensitive to both low- and high-frequency disturbances. For example, a change in room temperature induces thermal drifts typically requiring corrections of the order of minutes to hours. High-frequency disturbances that can be induced by acoustics or air turbulence are removed by averaging many individual measurements. Close to 100 measurements were typically averaged to achieve the required level of noise reduction.

A Windows-based desktop computer, with five extension slots, running at 2.5 GHz, was used to acquire interferometric data. The fringes were acquired with a monochrome CCD camera, internal to the ADE MiniFiz interferometer with RS-170 interface, and digitized with a four-channel, 8-bit data acquisition card from National Instruments, model 1409.[10] Processing artificial fringe patterns showed the numerical resolution of the software to be better than $\lambda/1000$. One channel of that card was used to digitize the image of the fringe pattern, while another channel was used to acquire a far-field view used for the diagnostic of the alignment.

The control loop was completed with three Picomotor controllers (New Focus 8753) (Ref. 8) that were driven by a hardware and software package. The Picomotors are digital stepping devices that move in nominal increments of 20 nm. The data acquisition and control software was developed with a rapid prototyping environment called BlackBox Component Builder,[11] which is available free of charge, and compiled with a Component Pascal compiler. The Blackbox environment is very robust and stable and well suited to developing mission-critical software, which requires a low occurrence of failures. An engineering and scientific software library[12] was used to perform matrix calculations and also for data logging and display. The library, written by Robert Campbell for the Blackbox environment, is distributed in source code.

The start-up sequence involves manual grating adjustments in two different positions. The grating assembly is rotated to be perpendicular to the interferometer axis, and both gratings, acting as mirrors, are co-aligned with respect to the Fizeau transmission flat to better than 1 μrad. This technique is referred to as "fringe-nulling." The grating assembly is then rotated to the Littrow position, where any measured differential vertical tilt is due to in-plane grating rotation. The fringe pattern is "nulled" with separate adjustments for both gratings to ensure that the grating grooves are parallel to one another. It may be necessary to reiterate these last two steps to make certain that the adjustments have settled and the adjusters are locked.

The reference transmission flat is now tilted to produce approximately 15 to 20 fringes across the field to enable the SSPD techniques to work with sufficient precision. Care must be taken to maintain wedge orientation within the interferometer and to maintain the same sign convention throughout the processing software. Once the manual setup steps are complete, the system is ready to perform open-loop stability measurements with the motors disabled. Alternatively, the control loop may be closed for precise grating control.

Experimental Results

The interferometric system was evaluated by measuring the differential phase between two regions of the same grating over an extended period of time. Each data point was acquired by averaging 16 sequential video frames. As shown in Fig. 100.24, an alignment variation of $\lambda/50$ rms was observed

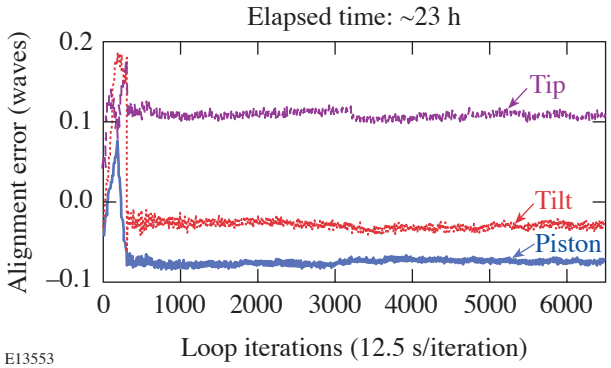

Figure 100.24
The stability of the phase sensor is evaluated by measuring the differential phase between two regions of a stable, monolithic grating. Long-term measurement of tip, tilt, and piston phase errors establishes the noise level of the system to be approximately $\lambda/50$. Statistical analysis, applied over time intervals of several minutes, reduces the measurement error to below $\lambda/100$. Extraneous fluctuations prior to sample 300 are reduced by applying temporal averaging in the SSPD routine.

over this period. Statistical analysis, applied over time intervals of several minutes, reduces the measurement error to below $\lambda/100$. Extraneous fluctuations prior to sample 300 were reduced by applying temporal averaging in the SSPD routine. After replacing the single grating with two gratings, phase measurements were made in open-loop mode over a 24-h period. As shown in Fig. 100.25, long-term monitoring of a TGA, with disabled actuators, indicates tip and tilt stability while the differential piston drifts by more than the wavelength of light. The system stability was found to vary by approximately five wavelengths of light per degree centigrade. The apparent phase jumps at $\pm\lambda/2$ are due to the $-\pi$ to π range of the arctangent calculation performed in phase reconstruction.

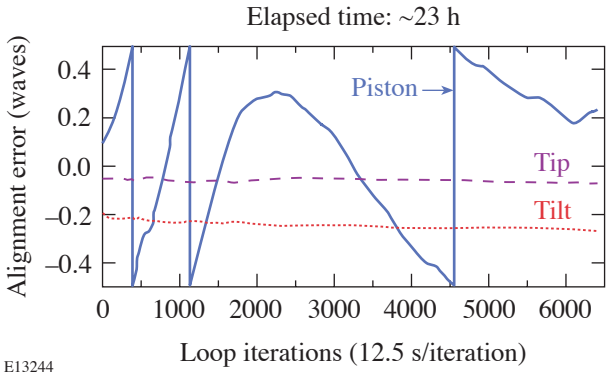

Figure 100.25
Long-term monitoring of a TGA, with disabled actuators, indicates tip and tilt stability while the differential piston drifts by more than the wavelength of light. The apparent phase jumps at $\pm\lambda/2$ are due to the $-\pi$ to π range of the arctangent calculation performed in phase reconstruction. The overall cyclical behavior of the piston term is caused by the difference in the coefficient of thermal expansion between the Pyrex™ substrate and aluminum mount in the presence of small temperature changes in the environment.

As a result of the phase-pair compensation strategy, any drift in either "*y* tip" or "in-plane grating rotation" is contained in the vertical "tilt signal," and their sum can be corrected with the servo system. Similarly, any drift in longitudinal shift (piston) or lateral shift is contained in the "piston signal," and their sum can be corrected by the servo system. A temperature recording, and subsequent analysis, showed that the cyclical behavior of the piston term is caused by the difference in the coefficient of thermal expansion between the Pyrex™ substrate and the aluminum mount in the presence of small temperature changes in the environment. The largest dimensions of the assembly are the widths of the gratings and the support structure. Since changes of these dimensions, due to temperature variation, are different for dissimilar materials, a phase shift occurs between the sets of grooves from their respective grating.

Closed-loop control of a TGA is achieved by driving the actuators with signals derived from the phase sensor. Phase fluctuations (Fig. 100.26) were largely reduced when the actuators were activated at sample number 9, and $\lambda/10$ alignment was rapidly achieved at sample number 25. As marked by sudden shifts in the plots, differential piston occurred at sample numbers 52 and 142. Tip and tilt phase correction was not required over the same time period. At the end of closed-loop operation, piston corrections in one-step increments, or 20 nm, are observed. This is comparable to the operation with a single grating where the far-field signal approximates a steady Airy pattern, with a Strehl ratio of about 0.99. During operation of an OMEGA EP laser beam, closed-loop control of up to eight interfaces will be required.

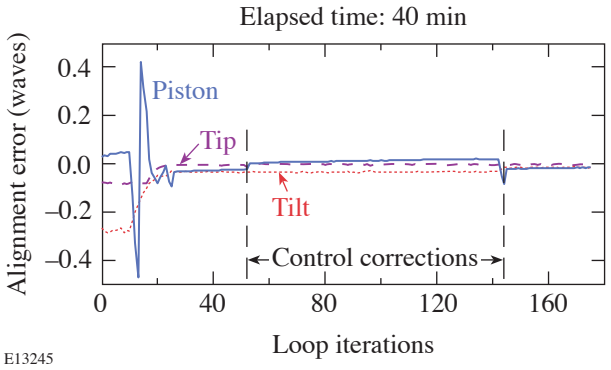

Figure 100.26
Closed-loop control of a TGA is achieved by enabling the actuators with signals derived from the phase sensor. Phase fluctuations were largely reduced when the actuators were enabled at sample number 9, and $\lambda/10$ alignment was achieved at sample number 25. As marked by sudden shifts in the plots, differential piston occurred at sample numbers 52 and 142. Tip and tilt phase correction was not required over the same time period.

An important demonstration of closed-loop control of the TGA involved obtaining convergence of all of the measured differential phase errors to zero following random offsets to the actuators [Fig. 100.27(a)]. Both the focal-spot irradiance and computed Strehl ratio tracked very well with the recorded differential piston. A focal spot splits into two lobes for a piston error of $(2N+1)\pi$ [Fig. 100.27(b)], while an Airy pattern [Fig. 100.27(c)] is recovered as the piston misalignment returns to near zero: For this experimental demonstration, the irradiance doubled after successful closed-loop alignment

[Figs. 100.27(d) and 100.27(e)]. A closed-loop run, requiring correction of initial tip, tilt, and piston errors, is completed in approximately 5 min. The settling time depends on the severity of the initial misalignments.

Operational ease can be achieved for closed-loop control of a tiled-grating compressor (TGC) through simultaneous alignment of all TGA's in a series configuration. Series alignment was demonstrated by positioning two TGA's in double-pass configuration using an auxiliary retroreflecting mirror. While one TGA was intentionally misaligned with a piston error of π radians [Fig. 100.28(a)], the second TGA was adjusted to remove all piston error from the series configuration [Fig. 100.28(b)]. Closed-loop alignment was successful despite an increase in diffraction losses due to the cumulative phase errors of the eight diffraction gratings. For comparison, a single TGA, in Littrow configuration, was alternately adjusted to form either a split focal spot [Fig. 100.28(c)] or a diffraction-limited focal spot [Fig. 100.28(d)].

Monochromatic laser light, operating at the center wavelength of a typical high-intensity laser, was used to simulate in-series alignment of the TGA units for the outer spectral components of broadband laser light. Figure 100.29(a) shows an experimentally generated phase map with the left and right regions of the beam accurately tiled, even though the individual TGA's are not properly tiled. Due to a spatial chirp that forms in part of the compressor, the extreme spectral components of the laser pulse cannot be fully compensated. The central, narrow region of the beam is not compensated and contained a differential tip of about three waves. The focal spot [Fig. 100.29(b)] shows a corresponding increase in diffraction

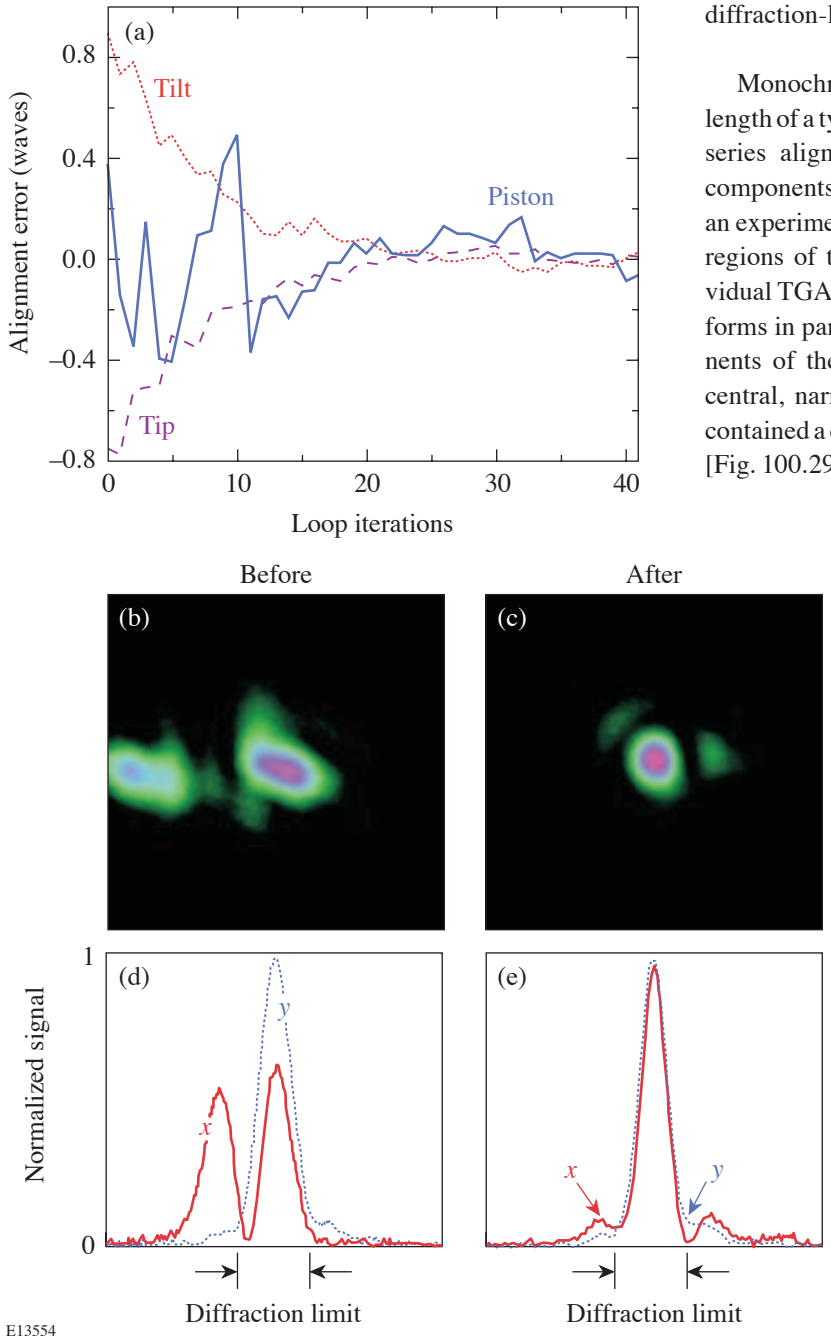

Figure 100.27
Closed-loop control of the TGA is achieved when all of the measured differential phase errors converge to zero following random offsets of the actuators (a). Corroboration between phase convergence and Strehl ratio indicates successful closed-loop control. A symmetrically split far-field pattern is observed for piston values of $(2N+1)\pi$ (b), while a single focal spot is observed for piston values of 0 and $2\pi n$ (c). The irradiance is doubled after successful alignment [(d) and (e)].

spreading in the horizontal plane due to the misregistration of the gaps. Diffraction spreading in the vertical plane is due to the differential tip of the central strip of light.

Theoretical calculations predict that integration over all spectral components of the laser pulse, carried through a TGC that is aligned with compensating TGA errors, yields negligible effects for pulses longer [Figs. 100.30(a) and 100.30(b)] than the Fourier-transform–limited ($\Delta\tau$) pulse [Fig. 100.30(c)]. Two-dimensional, space-time images clearly show that the effects from residual compensation error are pronounced only when maximum pulse compression is attempted. Further spatial integration of these images yields temporal pulses shapes [Fig. 100.30(d)] that show the small effect from a compensated π piston error in a pair of TGA units. Further modeling will be carried out to explore the combined effects of differential tip, tilt, and piston differential errors when in-series alignment is deployed.

Conclusion

Accurate closed-loop control of a tiled-grating assembly has been achieved over extended periods of time. Together with previous demonstrations involving coherent addition and pulse compression, this result further supports the feasibility of the tiled-grating compressor as the means to obtain multikilojoule-energy capability for petawatt-class lasers. In addition, in-series TGA alignment was successfully demonstrated in a compressor configuration.

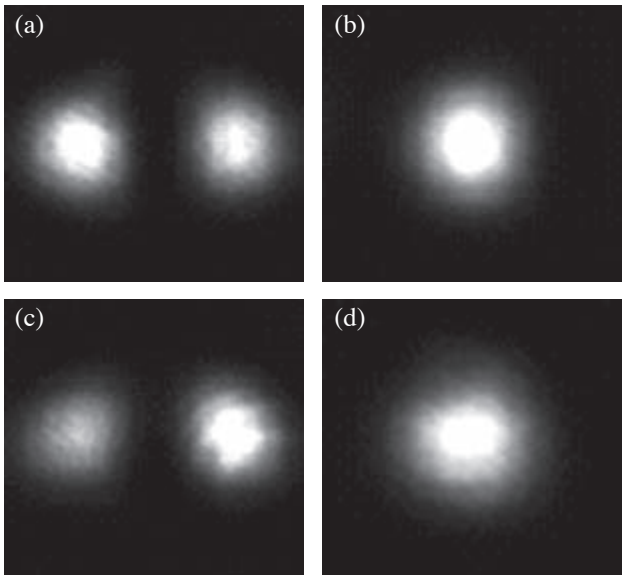

Figure 100.28
Operational ease can be achieved for closed-loop control of a tiled-grating compressor (TGC) through simultaneous alignment of all TGA's in series configuration. Series alignment was demonstrated by positioning two TGA's in double-pass configuration using an auxiliary retroreflecting mirror. While one TGA was intentionally misaligned with a piston error of π radians (a), the second TGA was adjusted to remove all piston error from the series configuration (b). Closed-loop alignment was successful despite an increase in diffraction losses due to the cumulative phase errors of the eight diffraction gratings. For comparison, a single TGA, in Littrow configuration, was alternately adjusted to form either a split focal spot (c) or a diffraction-limited focal spot (d).

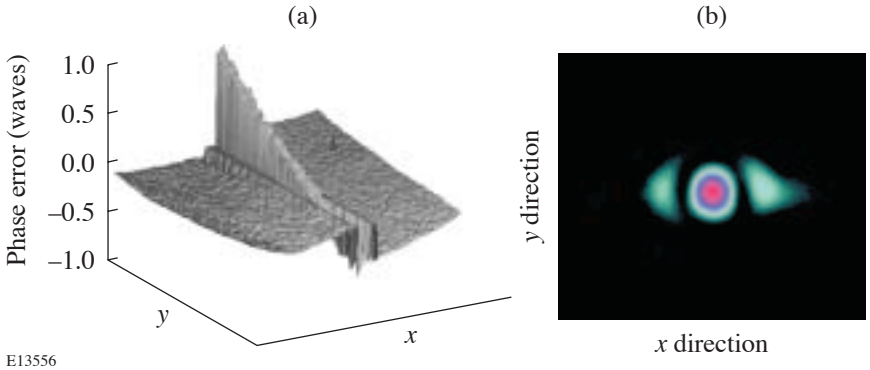

Figure 100.29
Monochromatic laser light was used to simulate in-series alignment of the TGA's for the outer-spectral components of broadband laser light. An experimentally generated phase map is shown in (a) with the left and right regions of the beam accurately tiled, even though the individual TGA's are not properly tiled. The central, narrow region of the beam is not compensated and contains a differential tilt of about three waves. The focal spot (b) shows a corresponding increase in diffraction spreading.

Further developments of the tiled-grating compressor are required to support the OMEGA EP project. A TMA with three tiled gratings is being constructed and tested to demonstrate full-aperture mounting, positioning, and closed-loop control. In addition, this prototype test apparatus will be outfitted with three full-aperture, MLD gratings to demonstrate phase-pair compensation and closed-loop control. Major emphasis will be placed on determining the minimum beam size required to accurately align a TGA containing three gratings using both near-field phase and far-field irradiance diagnostics.

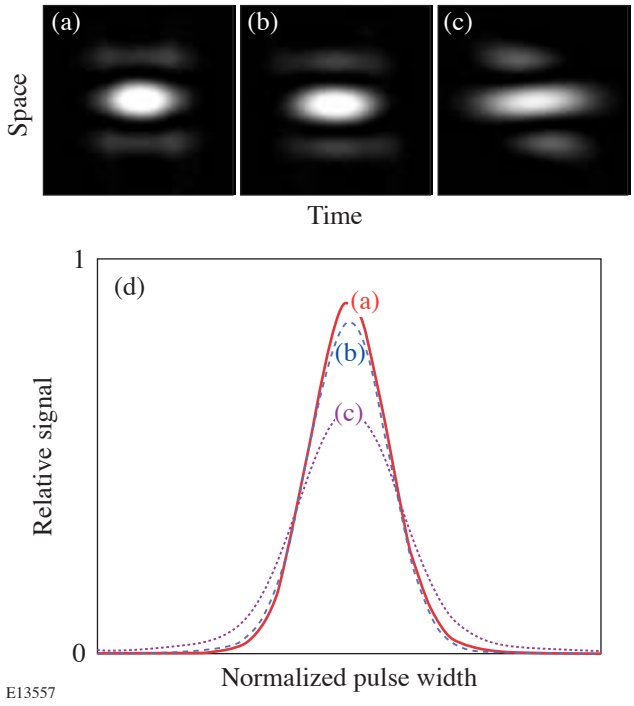

Figure 100.30
Theoretical calculations predict that integration over all spectral components of the laser pulse, carried through a TGC that is aligned with compensating TGA errors, yields negligible effects for pulses longer [(a) and (b)] than the Fourier-transform–limited ($\Delta\tau$) pulse (c). Two-dimensional, space-time images clearly show that the effects from residual compensation error are pronounced only when maximum pulse compression is attempted. Spatial integration of these images yields temporal pulse shapes (d) that show a relatively small effect.

ACKNOWLEDGMENT

This work was supported by the U.S. Department of Energy Office of Inertial Confinement Fusion under Cooperative Agreement No. DE-FC52-92SF19460, the University of Rochester, and the New York State Energy Research and Development Authority. The support of DOE does not constitute an endorsement by DOE of the views expressed in this article.

REFERENCES

1. T. J. Kessler, J. Bunkenburg, H. Huang, A. Kozlov, and D. D. Meyerhofer, Opt. Lett. **29**, 635 (2004).
2. Laboratory for Laser Energetics LLE Review **96**, 207, NTIS document No. DOE/SF/19460-509 (2003). Copies may be obtained from the National Technical Information Service, Springfield, VA 22161.
3. B. W. Shore *et al.*, J. Opt. Soc. Am. A **14**, 1124 (1997).
4. 2003 MLD Bulletin, Jobin Yvon, Inc., Gratings and OEM Division, Edison, NJ 08820-3012 (2003).
5. T. J. Kessler, J. Bunkenburg, and H. Huang, "Grating Array Systems for the Alignment and Control of the Spatial and Temporal Characteristics of Light," U.S. Patent Application (filed May 2003).
6. M. Born and E. Wolf, *Principles of Optics: Electromagnetic Theory of Propagation, Interference and Diffraction of Light*, 5th ed. (Pergamon Press, Oxford, 1975).
7. J. Bunkenburg, T. J. Kessler, H. Hu, C. Kellogg, and C. Kelly, presented at CLEO 2003, Baltimore, MD, 1–6 June 2003.
8. New Focus, Inc., a division of Brookham, http://www.newfocus.com (2004).
9. M. Takeda, H. Ina, and S. Kobayashi, J. Opt. Soc. Am. **72**, 156 (1982).
10. National Instruments, Austin, TX 78759-3504, http://www.ni.com (2004).
11. Oberon Microsystems, BlackBox Component Builder, available free of charge from http://www.oberon.ch./blackbox.html (2004).
12. R. Campbell, Engineering and Scientific Library for BlackBox Component Builder, available free of charge from http://www.zinnamturm.de/#Chill (2004).